

Time-Scaling in Atomistics and the Rate-Dependent Mechanical Behavior of Nanostructures

Xin Yan

Department of Mechanical Engineering, University of Houston, Houston, Texas 77004, United States

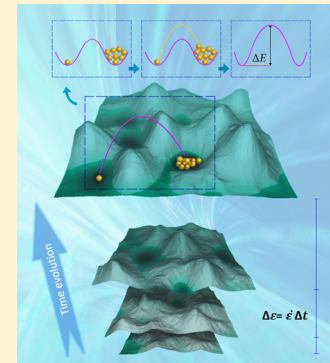
Pradeep Sharma*

Department of Mechanical Engineering, Department of Physics, and Material Science and Engineering Program, University of Houston, Houston, Texas 77004, United States

 Supporting Information

ABSTRACT: Conventional molecular dynamics simulations enable the elucidation of an astonishing array of phenomena inherent in the mechanical and chemical behavior of materials. Unfortunately, current computational limitations preclude accounting for processes whose transition times exceed, at best, microseconds. This limitation severely impacts, among others, a realistic assessment of slow-strain-rate mechanical behavior. In this work, using a simple paradigmatic model of a metallic nanopillar that is often the subject of experimental works, we attempt to circumvent the time-scale bottleneck of conventional molecular dynamics and provide novel physical insights into the rate-dependence of mechanical behavior of nanostructures. Using a collection of algorithms that include a recently developed potential energy surface sampling method—the so-called autonomous basin climbing approach, kinetic Monte Carlo, and others, we assess the nanopillar mechanical behavior under strain rates ranging from 1 to 10^8 s^{-1} . While our results for high-strain rate behavior are consistent with conventional molecular dynamics, we find that the response of nanostructures to slow compression is “liquid-like” and accompanied by extensive surface reconstructions.

KEYWORDS: Atomistic simulations, time scaling, rate dependence, mechanical behavior, nanostructures



The mechanical behavior of nanostructures is of significant interest both from a basic-science viewpoint as well as for its increasing relevance in applications that range from next-generation electronics and sensors to biomedical technology.^{1–3} This has inspired an exciting array of experimental studies that purport to understand how the mechanical behavior of nanostructures differ from bulk.^{4–6} An often-used paradigm is to mechanically compress a nanopillar and observe (*in situ*) its deformation.^{7–10} Complementary to these experimental studies, extensive work has also followed on using conventional molecular dynamics (MD) to obtain insights into the mechanisms underpinning the mechanical behavior of nanostructures.^{11–13} While the aforementioned modeling works have provided interesting insights, there is a fundamental limitation of conventional MD methodology that precludes an assessment of material behavior over realistic laboratory-time-scales. Molecular dynamics can only handle time-scales of the order of, at best, a few microseconds. While this is adequate for understanding several physical, chemical, and mechanical phenomena in materials, the inability to address long time-scales prevents an assessment of slow-strain rate mechanical behavior that is the norm in laboratory experiments and real-life applications. This shortcoming thus prevents an atomistically faithful understanding of phenomena like creep, void nucleation, defect migration, microstructure evolution, corro-

sion, and in general, most processes that are strongly *rate-dependent*.

In this Letter, inspired by (at least the partial) success of some recent work on bridging time-scales c.f.,^{14–18} we employ a collection of algorithms that assess the mechanical behavior of two-dimensional nanopillars¹⁹ under strain rates ranging from 1 to 10^8 s^{-1} . We note that conventional MD can only handle strain rates of 10^7 s^{-1} ²⁰ and higher, while our goal is to understand what truly happens in nanostructures at rates comparable to those found in the laboratories and applications (i.e., strain rates comparable to 1 s^{-1}). We choose a nickel nanoslab as the model material system although the goals of this Letter are not to communicate insights into any one particular material but rather proffer broader physical conclusions that pertain to capturing rate effects with atomistic fidelity. Furthermore, another motivation for choosing this particular system is that in a recent work, Pattamatta et al.²¹ precisely studied this configuration using an approach that is quite different than ours and thus presents an opportunity for a constructive comparison.

Received: January 9, 2016

Revised: May 10, 2016

Published: May 11, 2016

Consistent with ref 21, one of our model systems is a 116 atom Ni nanoslab. The simulation layout is depicted in Figure 1. The $x-y$ dimensions are $12.5 \times 35 \text{ \AA}$. The system is periodic

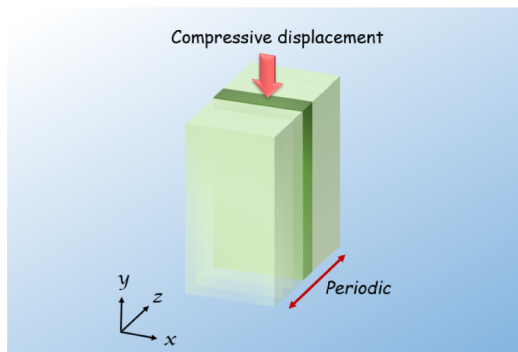


Figure 1. Schematic of the model studied in this work: compression of a two-dimensional nanopillar or a nanoslab at a given constant strain rate. The compressive loading is in the y -direction. Periodic boundary conditions are applied in the z -direction—hence the label of “two dimensional” nanopillar.

in the z -direction—hence the label of “two-dimensional” nanopillar.²² The z -direction unit-cell length is 2.46 \AA (Figure 1). Later, to investigate size effects, we will also consider a larger system size. The top and bottom layers are constrained to apply compressive displacement. A compression with constant strain-rate is applied to the system in the y -direction. The modified embedded-atom method (MEAM) potential is used in all of the calculations presented in this work.^{23,24} Further discussion on the effect of the choice of potentials can be found in Section V of the Supporting Information document.

General Overview and the Key Ingredients of the Time-Scaling Approach. A brief synopsis of our approach and the key ingredients of the time-scaling approach used by us is depicted in Figure 2 and briefly described below. Further details of this approach, including a flow-chart of the algorithm, may be found in Sections I and II of the Supporting Information document.

(i) We first fix the strain rate at which we wish to perform the simulation. The strain is then applied to the system in very small discrete steps, and we identify multiple potential energy surfaces (PES') corresponding to these very small strain steps. The PES during each small strain increment is identified by using the so-called autonomous basin climbing (ABC) algorithm described next.

(ii) *Sampling of the potential energy surface:* For a given set of boundary conditions (i.e., strain increment), the ABC algorithm^{14,25} is used to sample the PES. This determines the minima of the PES as well as the saddle points yielding thus the energy barriers between different local minima. The 3N-dimensional PES is quite complex indeed, and Figure 2 is merely a schematic representation to provide intuition to the reader. The ABC algorithm was proposed by Kushima and co-workers,^{14,25} and it has found success in a variety of contexts ranging from creep dislocation climb to void nucleation.^{26–28} In this approach, an energy minimized initial structure is activated by adding a penalty energy $\Phi_p^k(r)$ followed by subsequent relaxation. Usually, the penalty energy is in the form of a Gaussian function:

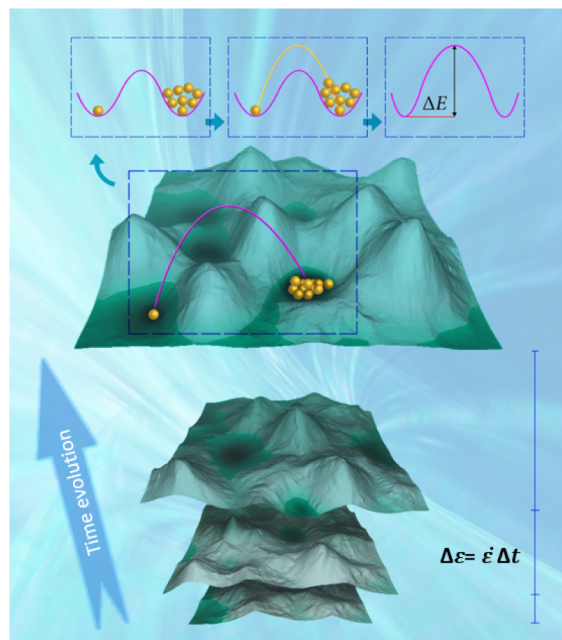


Figure 2. This figure describes the key ingredients behind the time-scaling approach used in this work. The corrugated surfaces represent the PES under different strains identified by the ABC algorithm. The main text and Sections I and III of the Supporting Information document describe how the strain rate is imposed and provide further details about the simulations.

$$\Phi_p^k(r) = \omega \exp[-(r - r_{\min}^k)/2\sigma^2] \quad (1)$$

centered at the minimum configuration r_{\min}^k . The parameters ω and σ control the shape and size of the penalty function. Through repeated application of the penalty imposition and the relaxation process, the system is pushed to climb up the basin to a higher energy configuration. In this manner, the algorithm outputs the configurations that the system visits successively, moving from one energy basin to another through energy activation and relaxation steps as shown in the left inset of Figure 2. We have implemented a parallel version of this algorithm in the LAMMPS software.²⁹ The size of the penalty should not be too large so that physically meaningful potential wells are not missed, nor too small that too many iterations are required to climb the barriers and obtain a “reasonable” sampling of the PES. Further details can be found in the following papers: refs 14 and 25. Needless to say, the sampling of a system of even a few hundred atoms is computationally demanding. Further details regarding the computational cost of our entire approach may be found in Section IV of the Supporting Information document. Recently, Park and co-workers,^{16,30} have modified the ABC approach so that the system adapts the penalty function parameters through a self-learning process.

(iii) *Minimum energy pathway for accurate determination of the energy barriers:* With a suitable penalty size and long-enough sampling time, in principle, the ABC algorithm can provide a “reasonable” approximation of the PES. Although the local minima are indeed captured accurately, unless the penalties are very small, the energy barriers are overestimated. Thus, to improve the accuracy of the energy barrier estimates, smaller penalties should be applied. However, this strategy is accompanied by a significant computational cost. Alternatively, the nudged elastic band (NEB),^{31,32} finite temperature string

(FTS)³³ or other such methods can be applied to the output of the ABC to obtain the minimum energy pathway between the initial minimum and all the possible final minima identified in ABC sampling.

(iv) *Kinetic Monte Carlo* (KMC): In ABC sampling, the accumulated penalties push the system to a neighboring minimum and prevent its return to any prior minima that has already been visited. To select the most probable path a system may take starting from some initial minimum state to all the minima identified in ABC, we apply KMC.³⁴ More details about application of KMC is described in Section III of the Supporting Information document.

(v) *Transition State Theory* (TST): With the barrier of the selected transition in hand, TST can be applied to calculate the transition time. In this work (like many others), we have used the so-called harmonic approximation of the TST, which can be expressed as

$$\Delta t = (\nu \exp[-\Delta E/k_b T])^{-1} \quad (2)$$

In the equation above, ν is the hopping frequency taken to be 10^{13} s⁻¹, and T is temperature (300 K for this work). The reader is referred to an interesting study by Nguyen et al.,³⁵ which illustrates the shortcomings of the harmonic TST. However, as will become evident in due course, numerical inaccuracy in the calculation of the precise time between events is not likely to impact the physical conclusions of this particular work since the time calculation is controlled through the way we impose the strain rate (please see remark below along with Section I of the Supporting Information document).

Remark on the Time Calculation and Imposition of Strain Rate. To avoid confusion in the readers mind about our approach, we make a few remarks about past literature as well as the calculation of time and imposition of strain rate in our work. The original ABC-based time-scaling proposal was simply a sampling technique. There is no way in that approach to perform a strain-rate controlled test. The original ABC-based approach identifies various minima and saddle points in the PES. The barriers are corrected by using NEB and then KMC is used to evolve the system. Finally, the transition state theory is used to complete the calculations by estimating the time taken between states.²⁷ We emphasize again that this approach²⁷ cannot be used to impose a fixed strain rate. In fact, large errors in the time-estimation can appear. In our work, while we do apply the ABC sampling algorithm to identify minima and saddle points, we do not calculate the time in the manner described in the preceding sentences. In our work, based on ref 15, we first fix the strain rate at which we wish to perform the simulation. The strain is applied to the system in very small discrete steps, and we identify multiple PES's corresponding to these very small strain steps. ABC sampling is then carried out for each of these discrete strain steps. We calculate the total time from the total deformation (strain ϵ) and the constant strain rate ($\dot{\epsilon}$) we have defined through the relation $t = \epsilon/\dot{\epsilon}$. This provides a fairly tight control over the transition time between minima if the strain increments are "small enough". In this work, to ensure this, indeed such small increments (for example $\Delta\epsilon < 5 \times 10^{-3}$) were applied to the system during each iteration (strain increment).

To benchmark the approach, we first consider a high strain rate of 1×10^8 s⁻¹ and compare the results with both conventional MD simulations and the Quenched Dynamics (QD) result from ref 21. Pattamatta et al.²¹ use a rather interesting approach for time-scaling based on bifurcation

theory (referred to as the Equilibrium Mapping (EM) approach). The deformation of the structure is shown in Figure 3, and our results (based on ABC, Figure 3a,

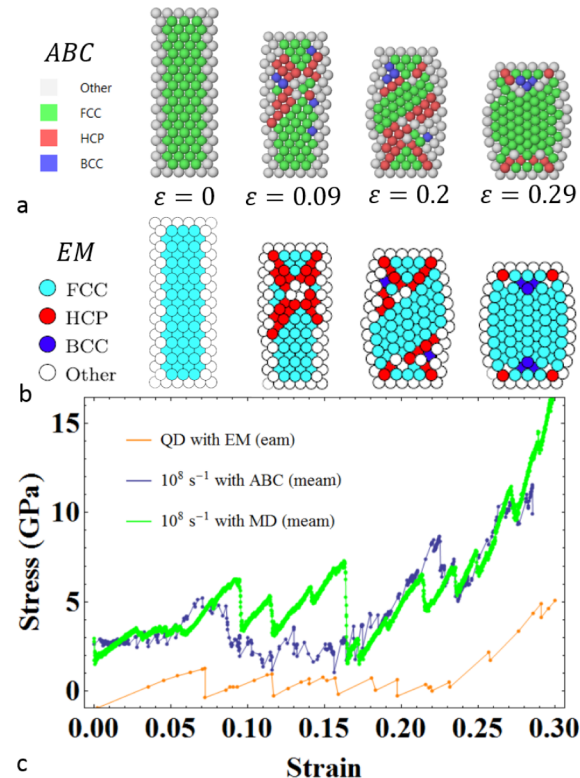


Figure 3. (a) High strain rate compression of Ni nanoslab using ABC and (b) the QD case of the EM approach from ref 21 are qualitatively similar. (c) Stress–strain behavior comparison between ABC, EM, and conventional MD. All three approaches exhibit the same trends. See Supplementary Videos S1 and S3 for the full evolution of deformation predicted by the ABC and MD approaches.

Supplementary Video S1) are compared with those of ref 21 the QD process (Figure 3b). Both methods start from the same initial structure (left snapshots)—a fcc nanoslab. Under the compression, X-shaped shear band appears in the nanoslab (snapshots of $\epsilon = 0.09$ in Figure 3a and b). In the central region of the nanoslab, the crystallographic orientation rotates by 90° and maps the original {110} free surfaces (in the x direction) on to {001}. The rotation of the crystallographic orientation pushes the X-shaped shear band to the top and bottom surfaces of the nanoslab (see the third snapshot in Figure 3a and b), and finally a barrel-shaped nanoslab is formed (snapshots of $\epsilon = 0.29$ in Figure 3a and b). A comparison between Figure 3a and b shows that the deformation sequence and patterns predicted by our approach and that of ref 21 are qualitatively similar. We have also carried out conventional MD simulations of this same structure (Supplementary Video S3), and those results also match ours (Supplementary Video S1). The resulting stress–strain behavior is shown in Figure 3c. Our result (blue line) is consistent with conventional MD (green line). In summary, for the case of the high strain rate (1×10^8 s⁻¹) accessible by conventional MD, our approach yields results that are consistent with both MD and those predicted by Pattamatta et al.²¹

We now turn to the key objective of this work—imposition of low-strain rates that are inaccessible by conventional MD.

For this case-study, we impose a strain rate of 1 s^{-1} . We remark that, in ref 21, predicated on the EM method, this particular simulation case was stopped at $\varepsilon = 0.08$. The ensuing deformation (Figure 4) under slow compression is remarkably

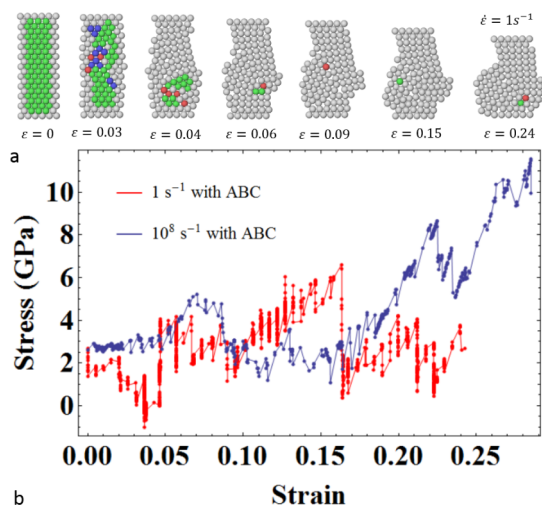


Figure 4. (a) Structure evolution of compression Ni nanoslab at low strain rate: $\varepsilon = 0$, initial fcc structure; $\varepsilon = 0.03$, the appearance of dislocation; $\varepsilon = 0.04$, amorphization starts from the top and bottom surface of the nanoslab; $\varepsilon = 0.06$, structure extends from free surfaces; $\varepsilon = 0.09$, structure extrusion with surface reconstruction; $\varepsilon = 0.15$, “liquid-like” deformation; $\varepsilon = 0.24$, some of atoms flow out of the simulation box. (b) Comparison of stress–strain behavior at high/low strain rates.

different from the high-strain rate case. The deformation is irregular, and both amorphization and surface reconstruction, including extrusion at the sides, can be observed during compression. Starting from the same fcc nanoslab as the high strain rate case, amorphization starts from the top and bottom of the structure (snapshots of $\varepsilon = 0.03$ and $\varepsilon = 0.04$ in Figure 4a). At the strain value of 0.06, almost all the fcc character of the original slab structure disappears. With increasing compression, the structure eventually extrudes from the free

surfaces of the nanoslab accompanied by extensive surface reconstruction (snapshots of $\varepsilon = 0.09$ and $\varepsilon = 0.15$ in Figure 4a). The proportion of crystalline structure progressively reduces with increasing deformation. Compared to the controlled (barrel-shaped) deformation evident in the high strain rate case, the deformation response at the low strain rate is almost “liquid-like”. The difference of the responses of high/low strain rate is also quantified with the help of the corresponding stress–strain curves shown in Figure 4b.

To assess the effect of size on the deformation of the nanoslab, we also carried out a set of simulations on a larger nanoslab (shown in Figure 5). The size of the model has the same x/y ratio ($25 \times 70\text{ \AA}$) as the smaller model shown in Figure 3, and in the z direction, the thickness of the unit cell is 2.46 \AA . There are 399 free atoms and 21 atoms at the boundaries which are utilized to impose the requisite boundary conditions. As before, we imposed two different strain rates of $1 \times 10^8\text{ s}^{-1}$ and 1 s^{-1} . The resulting deformation sequences are shown in Figure 5 (Supplementary Video S4 and S5 for the cases of high and low strain rate). In the case of high strain rate (top row in Figure 5), similar to the smaller-size model, the nanoslab undergoes a series of deformation from the initial fcc structure ($\varepsilon = 0$), exhibits two different kinds of shear bands ($\varepsilon = 0.06$ and $\varepsilon = 0.08$), and generally shows a similar trend as the smaller model, culminating in the barrel-shaped deformation ($\varepsilon = 0.22$ and $\varepsilon = 0.25$). In sharp contrast, the behavior under low strain rate is considerably more irregular. From initial fcc structure, the system starts amorphization from surfaces to the central part of the nanoslab (snapshots of $\varepsilon = 0.01$ and $\varepsilon = 0.02$). As with the smaller model, extrusion of the material with surface reconstruction is also observed (snapshots of $\varepsilon = 0.03$ and $\varepsilon = 0.06$), and the slow-strain rate behavior is “liquid-like”. Referring to the inset of Figure 6c, the plot of the centrosymmetry parameter allows us to infer that the nanoslab center indeed remains crystalline.

In a recent study of sub-10 nm crystalline silver particles,³⁶ both experiment and simulations observe “liquid-like” deformation in which the shape evolution is dominated by adatom diffusion on the surface and the structure which is a few layers under the surface remains crystalline. The reported deforma-

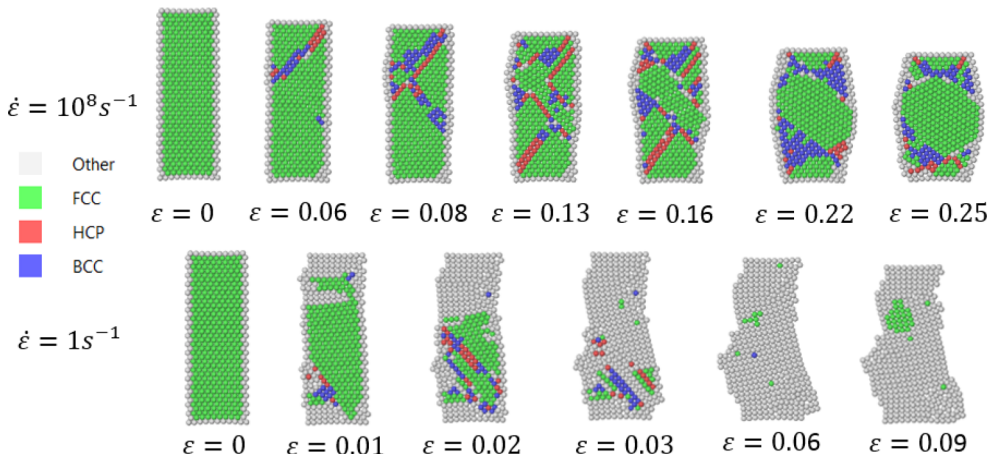


Figure 5. Structure evolution of larger Ni nanoslab under compression at high strain rate (top row) and low strain rate (bottom row). Both cases start from the same initial fcc structure and undergo a remarkably different evolution. For the case of high strain rate, the structure experiences the appearance of shear band ($\varepsilon = 0.06$ and $\varepsilon = 0.08$), the partially rotation of crystal orientation ($\varepsilon = 0.13$ and $\varepsilon = 0.16$), and a barrel-shaped structure ($\varepsilon = 0.22$ and $\varepsilon = 0.25$). For the case of low strain rate, amorphization starts from the top and bottom surfaces ($\varepsilon = 0.01$ and $\varepsilon = 0.02$) and is followed by material extrusion from the free surfaces ($\varepsilon = 0.03$ and $\varepsilon = 0.06$). However, the central region of the nanoslab remains crystalline ($\varepsilon = 0.09$).

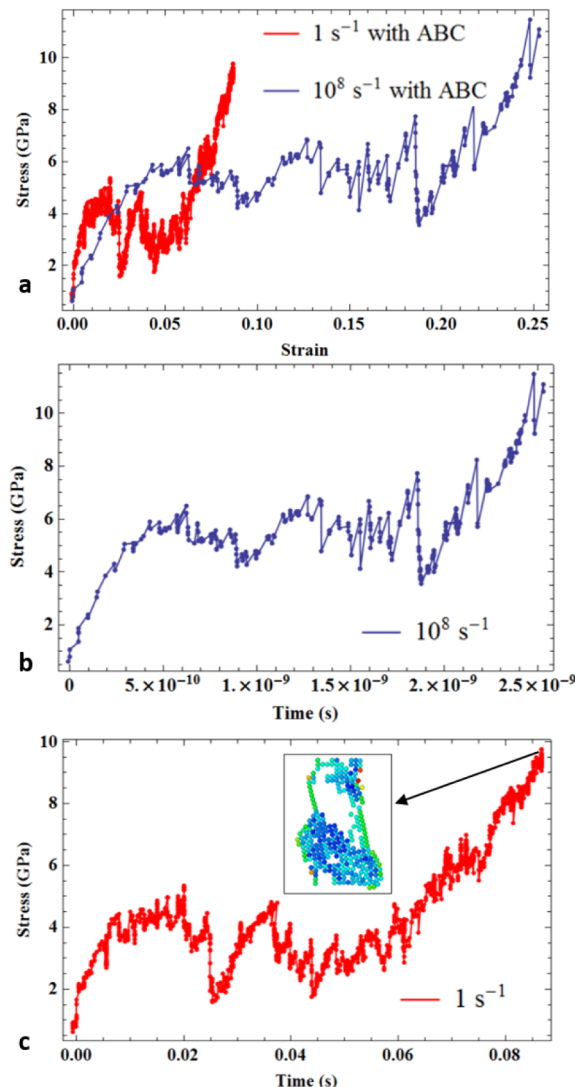


Figure 6. (a) Stress–strain curves for high/low strain rate for the large model; (b) stress versus time for high strain rate; (c) stress versus time for low strain rate and the inset shows the structure using the centrosymmetry parameter for low strain rate and at the strain value of 0.09.

tion is quite similar to what we observed in our simulations. We believe that the studied nanostructure deforms in a “liquid-like” deformation (at slow strain rates) because of the surface diffusion while the central interior part of it behaves more like a crystalline solid, as shown in the inset of Figure 6c. Further, a comparison of stress–strain curves shown in Figure 6a indicates that, for the case of low strain rate, hardening starts at the strain level of 0.07; however, for the case of high strain rate, the hardening may be observed at a much higher strain value of 0.2. In Figure 6b and c, we show stress versus time for both high strain rate and low strain rate cases. In our low strain rate simulations, a loading duration of 0.09 s is achieved—well in line with what may be observed in laboratory conditions. In contrast, for high strain rate, the total loading time is of the order of 10^{-9} s .

In summary, we have carried out a study of the mechanical compression behavior of nanoslabs to specifically interrogate its deformation behavior under both slow and fast strain rates. While high-strain rate deformation proceeds in an unremarkable manner—merely shortening its length along with the

formation of an expected defect substructure, the slow-strain rate results (precisely what is to be expected in most applications and laboratory experiments) exhibit a dramatically different behavior. We observe “liquid-like” deformation under low strain rate. In situ experiments³⁶ appear to qualitatively confirm our observations that nano structures, indeed, are more likely to exhibit the deformation pattern we have captured with the adopted time-scaling approach in sharp contrast to the predictions of conventional molecular dynamics.

■ ASSOCIATED CONTENT

S Supporting Information

The Supporting Information is available free of charge on the ACS Publications website at DOI: [10.1021/acs.nanolett.6b00117](https://doi.org/10.1021/acs.nanolett.6b00117).

I. Implementation of finite strain rate; II. Comparison of other ABC-based approaches; III. Simulation details; IV. Computational cost evaluation; V. Molecular dynamics (MD) simulations with different potentials ([PDF](#))

Deformation of the Ni nano-slab under compression at high strain rate (10^8 s^{-1}) using our approach ([AVI](#))

Deformation of the Ni nano-slab under compression at low strain rate (1 s^{-1}) using our approach ([AVI](#))

Deformation of the Ni nano-slab under compression at high strain rate (10^8 s^{-1}) using conventional MD ([AVI](#))

Deformation of the large Ni nano-slab under compression at high strain rate (10^8 s^{-1}) using our approach ([AVI](#))

Deformation of the large Ni nano-slab under compression at low strain rate (1 s^{-1}) using our approach ([AVI](#))

Deformation of the large Ni nano-slab under compression at high strain rate (10^8 s^{-1}) using conventional MD ([AVI](#))

■ AUTHOR INFORMATION

Corresponding Author

*E-mail: psharma@uh.edu.

Notes

The authors declare no competing financial interest.

■ ACKNOWLEDGMENTS

We gratefully acknowledge the support from NSF CMMI grants no. 1161163, no.1463205, the M.D. Anderson Professorship, and numerous helpful discussions with Drs. Yashashree Kulkarni and Xiaobao Li.

■ REFERENCES

- (1) Lee, M.-S.; Lee, K.; Kim, S.-Y.; Lee, H.; Park, J.; Choi, K.-H.; Kim, H.-K.; Kim, D.-G.; Lee, D.-Y.; Nam, S.; et al. *Nano Lett.* **2013**, *13*, 2814.
- (2) Rogers, J. A.; Someya, T.; Huang, Y. *Science* **2010**, *327*, 1603.
- (3) Park, M.; Im, J.; Shin, M.; Min, Y.; Park, J.; Cho, H.; Park, S.; Shim, M.-B.; Jeon, S.; Chung, D.-Y.; et al. *Nat. Nanotechnol.* **2012**, *7*, 803.
- (4) Gleiter, H. *Acta Mater.* **2000**, *48*, 1.
- (5) Biener, J.; Hodge, A. M.; Hayes, J. R.; Volkert, C. A.; Zepeda-Ruiz, L. A.; Hamza, A. V.; Abraham, F. F. *Nano Lett.* **2006**, *6*, 2379.
- (6) Greer, J. R.; Oliver, W. C.; Nix, W. D. *Acta Mater.* **2005**, *53*, 1821.
- (7) Aitken, Z. H.; Fan, H.; El-Awady, J. A.; Greer, J. R. *J. Mech. Phys. Solids* **2015**, *76*, 208.
- (8) Lee, S.-W.; Jennings, A. T.; Greer, J. R. *Acta Mater.* **2013**, *61*, 1872.

- (9) Guo, Q.; Landau, P.; Hosemann, P.; Wang, Y.; Greer, J. R. *Small* **2013**, *9*, 691.
- (10) Jennings, A.; Gross, C.; Greer, F.; Aitken, Z.; Lee, S.-W.; Weinberger, C.; Greer, J. *Acta Mater.* **2012**, *60*, 3444.
- (11) Weinberger, C. R.; Cai, W. *Proc. Natl. Acad. Sci. U. S. A.* **2008**, *105*, 14304.
- (12) Weinberger, C. R.; Cai, W. *Scr. Mater.* **2011**, *64*, 529.
- (13) Healy, C. J.; Ackland, G. J. *Acta Mater.* **2014**, *70*, 105.
- (14) Kushima, A.; Lin, X.; Li, J.; Eapen, J.; Mauro, J. C.; Qian, X.; Diep, P.; Yip, S. *J. Chem. Phys.* **2009**, *130*, 224504.
- (15) Fan, Y.; Ossetskiy, Y. N.; Yip, S.; Yildiz, B. *Proc. Natl. Acad. Sci. U. S. A.* **2013**, *110*, 17756.
- (16) Cao, P.; Lin, X.; Park, H. S. *J. Mech. Phys. Solids* **2014**, *68*, 239.
- (17) Yan, X.; Gousssem, A.; Sharma, P. *Mech. Mater.* **2015**, *91*, 306.
- (18) Gousssem, A.; Sarangi, R.; Deng, Q.; Sharma, P. *Comput. Mater. Sci.* **2015**, *104*, 200.
- (19) We will henceforth refer to these as “nanoslabs”.
- (20) Zhu, T.; Li, J.; Samanta, A.; Leach, A.; Gall, K. *Phys. Rev. Lett.* **2008**, *100*, 025502.
- (21) Pattamatta, S.; Elliott, R. S.; Tadmor, E. B. *Proc. Natl. Acad. Sci. U. S. A.* **2014**, *111*, E1678.
- (22) We remark that we are not solving a two-dimensional problem and some researchers may prefer the adjective “2.5 dimensional” to distinguish our model system from a real two-dimensional problem.
- (23) Baskes, M. *Phys. Rev. Lett.* **1987**, *59*, 2666.
- (24) Plimpton, S. J.; Thompson, A. P. *MRS Bull.* **2012**, *37*, 513.
- (25) Kushima, A.; Eapen, J.; Li, J.; Yip, S.; Zhu, T. *Eur. Phys. J. B* **2011**, *82*, 271.
- (26) Lau, T. T.; Kushima, A.; Yip, S. *Phys. Rev. Lett.* **2010**, *104*, 175501.
- (27) Fan, Y.; Kushima, A.; Yip, S.; Yildiz, B. *Phys. Rev. Lett.* **2011**, *106*, 125501.
- (28) Fan, Y.; Ossetsky, Y. N.; Yip, S.; Yildiz, B. *Phys. Rev. Lett.* **2012**, *109*, 135503.
- (29) Plimpton, S. J. *Comput. Phys.* **1995**, *117*, 1.
- (30) Cao, P.; Li, M.; Heugle, R. J.; Park, H. S.; Lin, X. *Phys. Rev. E* **2012**, *86*, 016710.
- (31) Henkelman, G.; Jonsson, H. J. *Chem. Phys.* **2000**, *113*, 9978.
- (32) Henkelman, G.; Uberuaga, B. P.; Jónsson, H. J. *Chem. Phys.* **2000**, *113*, 9901.
- (33) Ren, W.; Vanden-Eijnden, E. *J. Phys. Chem. B* **2005**, *109*, 6688.
- (34) Voter, A. F. In *Radiation Effects in Solids*; Springer, 2007; pp 1–23.
- (35) Nguyen, L.; Baker, K.; Warner, D. *Phys. Rev. B: Condens. Matter Mater. Phys.* **2011**, *84*, 024118.
- (36) Sun, J.; He, L.; Lo, Y.-C.; Xu, T.; Bi, H.; Sun, L.; Zhang, Z.; Mao, S. X.; Li, J. *Nat. Mater.* **2014**, *13*, 1007.